On electron heating, deposition rate, and ion recycling in the high power impulse magnetron sputtering discharge

Jón Tómas Guðmundsson[1,2]

[1]Division of Space and Plasma Physics,
KTH Royal Institute of Technology, Stockholm, Sweden
[2] Science Institute, University of Iceland, Reykjavik, Iceland

Department of Physics, University of West Bohemia,
Pilsen, Czech Republic
April 1, 2025

Introduction – Magnetron sputtering

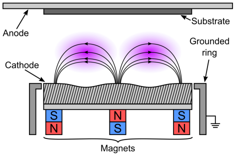

Gudmundsson and Lundin (2020) in High Power Impulse Magnetron Sputtering Discharge, Elsevier, 2020

- Magnetron sputtering has been a highly sucessfull technique that is essential in a number of industrial applications

  Gudmundsson (2020) PSST **29** 113001
- In a high power impulse magnetron sputtering (HiPIMS) the discharge is driven by high power pulses of low repetition frequency, and with low duty cycle
- This results in high discharge current density, increased electron density, and increased ionization of the sputtered species

  Gudmundsson et al. (2012) JVSTA **30** 030801

Overview

- The dc magnetron sputtering discharge
- The high power impulse magnetron sputtering discharge (HiPIMS)
- Thin film deposition
- Electron power absorption in magnetron sputtering discharges
- The ionization region model (IRM)
- Ionization region model studies of HiPIMS
- Deposition rate vs ionized flux fraction
- Working gas rarefaction
- Summary

The dc magnetron sputtering discharge

The dc magnetron sputtering discharge

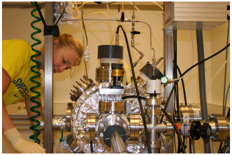

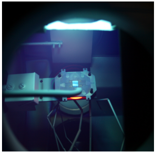

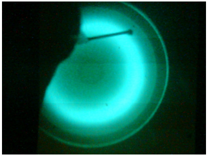

- Magnetron sputtering has been the workhorse of plasma based sputtering methods for over four decades
- Through the years there has been a continuous development of the magnetron sputtering processes to
  - increase the ionization of the sputtered species
  - improve target utilization
  - avoid target poisoning in reactive sputtering
  - increase deposition rates

The dc magnetron sputtering discharge

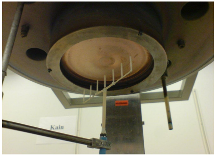
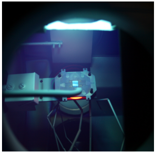
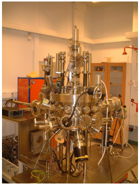

- For many applications a high degree of ionization of the sputtered species is desired
  - controlled ion bombardment of the growing film
  - ion energy can be – controlled by a negative bias applied to the substrate
  - collimation – enhanced step coverage

- Ionized flux of the sputtered material introduces an additional control parameter into the deposition process

The dc magnetron sputtering discharge

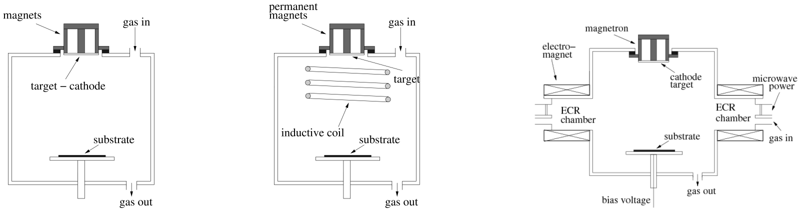

From Gudmundsson (2008), J. Phys.: Conf. Ser. **100** 082002

- In magnetron sputtering discharges increased ionized flux fraction is achieved by
  - a secondary discharge between the target and the substrate (rf coil or microwaves)
  - reshaping the geometry of the cathode to get more focused plasma (hollow cathode)
  - increasing the power to the cathode (high power pulse)
- Common to all highly ionized magnetron sputtering techniques is a very high density plasma

The high power impulse magnetron sputtering discharge (HiPIMS)

High power impulse magnetron sputtering discharge

- In a conventional dc magnetron discharge the power density is limited by the thermal load on the target
- Most of the ion bombarding energy is transformed into heat at the target
- In a HiPIMS discharge a high power pulse is supplied for a short period
  - low frequency
  - low duty cycle
  - low average power
- The high power pulsed magnetron sputtering discharge uses the same sputtering apparatus except for the power supply

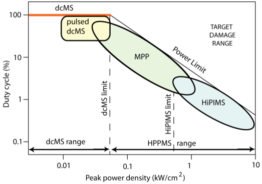

Power density limits

p_t = 0.05 kW/cm^2 dcMS limit

p_t = 0.5 kW/cm^2 HiPIMS limit

Gudmundsson et al. (2012) JVSTA **30** 030801

High power impulse magnetron sputtering discharge

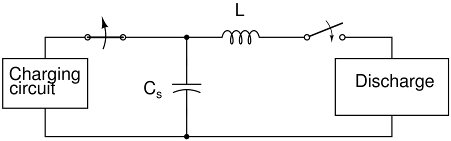

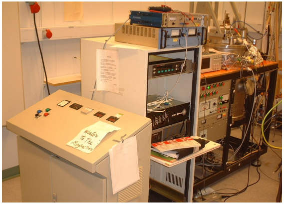

- The high power impulse magnetron sputtering (HiPIMS) discharge operates with a
  - Cathode voltage in the range of 500 – 2000 V
  - Current densities of 0.5 – 4 A/cm^2
  - Power densities in the range of 0.5 – 3 kW/cm^2
  - Average power 200 – 600 W
  - Frequency in the range of 50 – 5000 Hz
  - Duty cycle in the range of 0.5 – 5 %

High power impulse magnetron sputtering discharge

- In a **non-reactive** discharge the current waveform exhibits an initial pressure dependent peak that is followed by a second phase that is power and material dependent
- The initial phase is dominated by working gas ions, whereas the later phase has a strong contribution from self-sputtering
- For some materials, the discharge switches into a mode of **sustained self-sputtering**

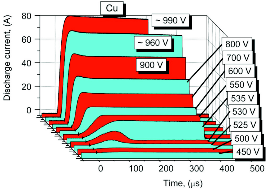

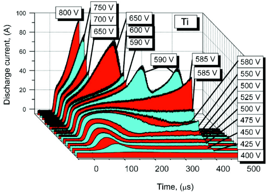

From Anders et al. (2007),

JAP **102** 113303 and JAP **103** 039901

High power impulse magnetron sputtering discharge

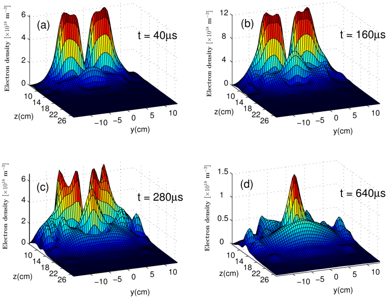

After Bohlmark et al. (2005), IEEE Trans. Plasma Sci. **33** 346

- Temporal and spatial variation of the electron density
- Ar discharge at 20 mTorr, Ti target, pulse length 100 μs
- The electron density in the substrate vicinity is of the order of $10^{18} - 10^{19}$ m^{-3} – ionization mean free path $\lambda_{iz} \sim 1$ cm

High power impulse magnetron sputtering discharge

- The time averaged ion energy distribution for Ar^+ and Ti^+ ions
- The working gas pressure was 3 mTorr, pulse energy 3 J and 10 J and the target made of Ti
- The ion energy distribution is broad to over 100 eV
- About 50 % of the Ti^+ ions have energy > 20 eV

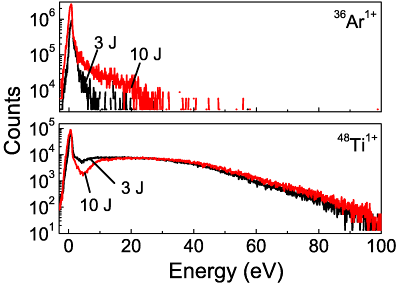

From Bohlmark et al. (2006) TSF **515** 1522

Thin film deposition

Thin film deposition

- The film mass density is always higher – when depositing with HiPIMS compared to dcMS at the same average power
- The surfaces are significantly smoother
- The films typically exhibit better crystallinity, and overall improved film properties
  - lower electrical resistivity
  - improved optical properties
  - improved mechanical properties
  - better oxidation resistance
  - higher hardness

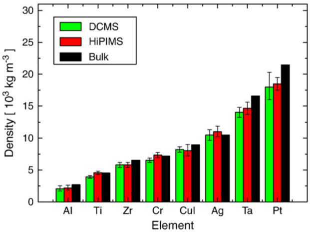

From Samuelsson et al. (2010) SCT **202** 591

Thin film deposition

- The effect of ionization fraction on the epitaxial growth of Cu film on Cu(111) substrate explored using Molecular Dynamics simulation
- Three deposition methods
  - thermal evaporation, fully neutral
  - dcMS, 50 % ionized
  - HiPIMS, 100 % ionized
- Higher ionization fraction of the deposition flux leads to smoother surfaces by two major mechanisms
  - decreasing clustering in the vapor phase
  - bicollision of high energy ions at the film surface that prevents island growth to become dominant

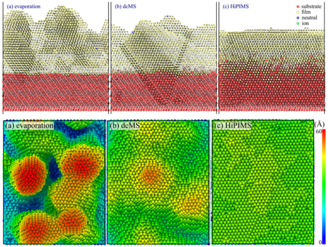

After Kateb et al. (2019) JVSTA, **37** 031306

Thin film deposition

- There is a drawback
- The deposition rate is lower for HiPIMS when compared to dcMS operated at the same average power
- The HiPIMS deposition rates are typically in the range of 30 – 85% of the dcMS rates depending on target material
- Many of the ions of the target material are attracted back to the target surface by the cathode potential

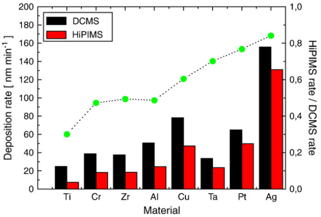

From Samuelsson et al. (2010) SCT **202** 591

Electron power absorption in magnetron sputtering discharges

Electron power absorption

- The conventional wisdom is that plasma generation in magnetron sputtering discharges is based on the supply of energy via secondary electrons (SEs) accelerated from the target
- However, one of the remaining fundamental questions is **how power is absorbed by the electrons in the magnetron sputtering discharge**

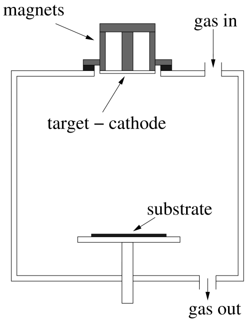

Electron power absorption

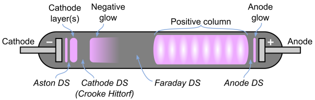

T. J. Petty, LPGP, Université Paris Sud

- A dc discharge with a cold cathode is sustained by secondary electron emission from the cathode by ion bombardment
- The discharge current at the target consists of electron current I_e and ion current I_i or

$$I_\mathrm{D} = I_\mathrm{e} + I_\mathrm{i} = I_\mathrm{i}(1 + \gamma_\mathrm{SE})$$

  where γ_SE is the secondary electron emission coefficient
- Note that $\gamma_\mathrm{SE} \sim 0.05 - 0.2$ for most metals, so at the target, the dominating fraction of the discharge current is ion current

Electron power absorption

- These secondary electrons are accelerated in the cathode dark space – referred to as primary electrons
- They must produce sufficient number of ions to release more electrons from the cathode
- The number of electron-ion pairs created by each secondary electron is then

$$\mathcal{N} \approx \frac{V_\mathrm{D}}{\mathcal{E}_\mathrm{c}}$$

where $\mathcal{E}_\mathrm{c}$ is the energy loss per electron-ion pair created

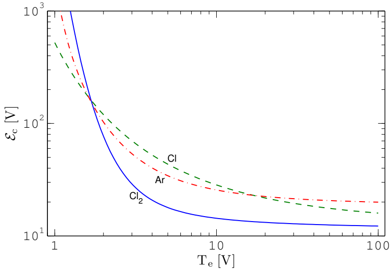

Electron power absorption

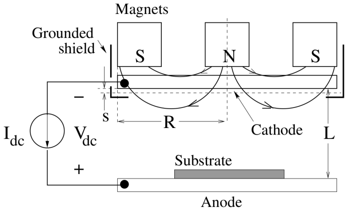

- To account for the electrons that are not trapped we define an effective secondary electron emission coefficient

$$\gamma_{\rm SE,eff} = m\epsilon_{\rm e}(1-r)\gamma_{\rm SE}$$

- $\epsilon_{\rm e}$ is the fraction of the electron energy that is used for ionization before being lost
- m is a factor that accounts for secondary electrons ionizing in the sheath
- r is the recapture probability of secondary electrons

Electron power absorption

- To sustain the discharge the condition

$$\gamma_{\rm SE,eff}\mathcal{N} = 1$$

has to be fulfilled

- This defines the minimum voltage to sustain the discharge as

$$V_{\rm D,min} = \frac{\mathcal{E}_{\rm c}}{\beta\gamma_{\rm SE,eff}}$$

referred to as Thornton equation

  - β is the fraction of ions that return to the cathode

Magnetron sputtering: basic physics and application to cylindrical magnetrons

John A. Thornton

Telic Corporation, 1631 Colorado Avenue, Santa Monica, California 90404

(Received 22 September 1977; accepted 7 December 1977)

Magnetron sputtering sources can be defined as diode devices in which magnetic fields are used in concert with the cathode surface to form electron traps which are so configured that the **E**×**B** electron-drift currents close on themselves. Coaxial cylindrical magnetron sputtering sources in which post or hollow cathodes are operated in axial magnetic fields have been reported for a number of years. However, their performance is limited by end losses. A remarkable performance is achieved when the end losses are eliminated by proper shaping of the magnetic field or by using suitably placed electron-reflecting surfaces. High currents and sputtering rates can be obtained, nearly independent of voltage, even at low pressures. This characterizes what has been defined as the *magnetron mode* of operation. This paper reviews the basic principles that underly the operation of dc sputtering sources in the magnetron mode with particular emphasis on cylindrical magnetrons. The important attributes of these devices as sputtering sources are also reviewed.

PACS numbers: 81.15.−z, 52.75.−d

Thornton (1978) JVST **15**(2) 171

Electron power absorption

- The basic assumption is that acceleration across the sheath is the main source of energy for the electrons
- Above breakdown the parmeters m, β, ϵ_{e} and r can vary with the applied voltage
- We can rewrite the Thornton equation for any voltage

$$\frac{1}{V_{\mathrm{D}}} = \frac{\beta m \epsilon_{\mathrm{e}}(1-r)}{\mathcal{E}_{\mathrm{c}}} \gamma_{\mathrm{SE}}$$

A low-pressure cold-cathode discharge is maintained primarily by secondary electrons emitted from the cathode by ion bombardment. These electrons are accelerated in the CDS and enter the plasma where, known as primary electrons, they must produce sufficient ions to release one further electron from the cathode.[72] This requirement can be expressed by the following relationship for the minimum potential to sustain such a discharge:[73]

$$V_{\min} = \mathcal{E}_0/\Gamma_i \epsilon_i \epsilon_e \qquad (5)$$

Thornton (1978) JVST **15**(2) 171

Electron power absorption

- A plot of the inverse discharge voltage $1/V_{\mathrm{D}}$ against γ_{SE} should then give a straight line through the origin
- Depla et al. measured the discharge voltage for a 5 cm diameter target for Ar working gas for 18 different target materials
- Since all the data is taken in the same magnetron sputtering discharge, at same current and pressure, the discharge parameters parmeters m, β, ϵ_{e} and $\mathcal{E}_{\mathrm{c}}$ are independent of γ_{SE}

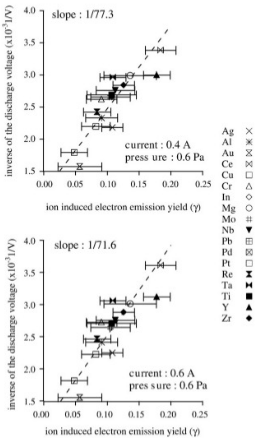

From Depla et al. (2009) TSF **517** 2825

Electron power absorption

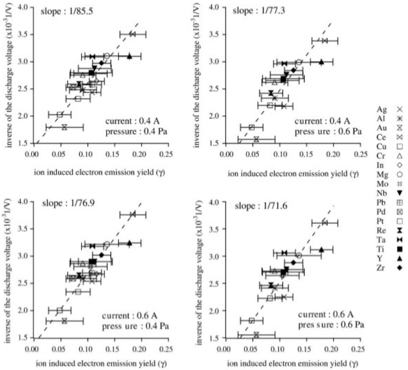

From Depla et al. (2009) TSF **517** 2825

- $1/V_{\rm D}$ against $\gamma_{\rm SE}$ for working gas pressures of 0.4 and 0.6 Pa and discharge currents 0.4 A and 0.6 A
- It can be seen that a straight line indeed results, but that it does not pass through the origin

Electron power absorption

- We here propose that the intercept is due to Ohmic heating
- We can now write the inverse discharge voltage $1/V_{\mathrm{D}}$ in the form of a generalized Thornton equation

$$\frac{1}{V_{\mathrm{D}}} = \underbrace{\frac{\beta\epsilon_{\mathrm{e}}^{\mathrm{H}} m(1-r)(1-\delta_{\mathrm{IR}})}{\mathcal{E}_c^{\mathrm{H}}}}_{a}\gamma_{\mathrm{SE}} + \underbrace{\frac{\epsilon_{\mathrm{e}}^{\mathrm{C}}\langle I_{\mathrm{e}}/I_{\mathrm{D}}\rangle_{\mathrm{IR}}\delta_{\mathrm{IR}}}{\mathcal{E}_c^{\mathrm{C}}}}_{b}$$

or

$$\frac{1}{V_{\mathrm{D}}} = a\gamma_{\mathrm{SE}} + b$$

- We associate a with hot electrons e^{H}, sheath acceleration
- We associate b with the Ohmic heating process and cold electrons e^{C}

Electron power absorption

- The figure shows schematically the magnetic field lines and the electric equipotential surfaces above the racetrack
- A potential V_{SH} falls over the sheath, and the rest of the applied voltage, $V_{\mathrm{IR}} = V_{\mathrm{D}} - V_{\mathrm{SH}}$, falls across the extended pre-sheath, the ionization region (IR), $\delta_{\mathrm{IR}} = V_{\mathrm{IR}}/V_{\mathrm{D}}$
- Ohmic heating, the dissipation of locally deposited electric energy $\mathbf{J}_{\mathrm{e}} \cdot \mathbf{E}$ to the electrons in the plasma volume outside the sheath

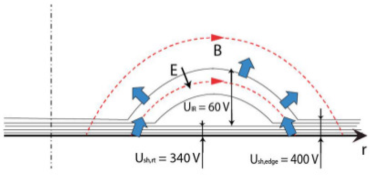

From Brenning et al. (2016) PSST **25** 065024

Electron power absorption

I_D (A)	p (Pa)	Slope k	Intercept I	$\delta_{IR} = U_{IR}/U_D$
0.4	0.4	0.0117	0.001 45	0.19
0.4	0.6	0.0129	0.001 20	0.16
0.6	0.4	0.0130	0.001 30	0.17
0.6	0.6	0.0140	0.001 10	0.15

- It follows that the fraction of the total ionization that is due to Ohmic heating can be obtained directly from the line fit parameters *a* and *b*
- This can be written as a function of only the secondary electron yield γ_{SE}

$$\frac{\iota_{\text{Ohmic}}}{\iota_{\text{total}}} = \frac{b}{a\gamma_{SE} + b}$$

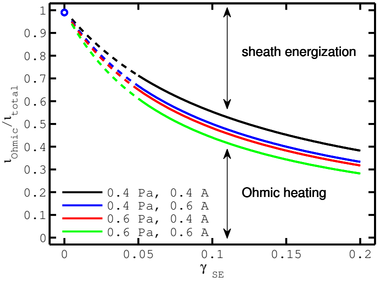

From Brenning et al. (2016) PSST **25** 065024

Electron power absorption

I_D (A)	p (Pa)	Slope k	Intercept l	$\delta_{IR} = U_{IR}/U_D$
0.4	0.4	0.0117	0.00145	0.19
0.4	0.6	0.0129	0.00120	0.16
0.6	0.4	0.0130	0.00130	0.17
0.6	0.6	0.0140	0.00110	0.15

- The fraction of the discharge voltage that falls over the ionization region

$$\delta_{\mathrm{IR}} = \frac{V_{\mathrm{IR}}}{V_{\mathrm{D}}}$$

can be estimated from

$$b = \frac{\epsilon_{\mathrm{e}}^{\mathrm{C}} \langle I_{\mathrm{e}}/I_{\mathrm{D}}\rangle_{\mathrm{IR}} \delta_{\mathrm{IR}}}{\mathcal{E}_c^{\mathrm{C}}}$$

- We assume

$$\epsilon_{\mathrm{e}}^{\mathrm{C}} = 0.8, \quad \langle I_{\mathrm{e}}/I_{\mathrm{D}}\rangle_{\mathrm{IR}} \approx 0.5,$$

and

$$\mathcal{E}_c^{\mathrm{C}} = 53.5 \text{ V} \quad \text{for} \quad T_{\mathrm{e}} = 3 \text{ V}$$

which gives

$$\delta_{\mathrm{IR}} = 0.15 - 0.19$$

- 15 - 19 % of the applied discharge voltage falls over the ionization region

Electron power absorption

- Recent measurements have revealed strong electric fields parallel and perpendicular to the target of a dc magnetron sputtering discharge
- The largest **E**-fields result from a double layer structure at the leading edge of an ionization zone
- It is suggested that the double layer plays a crucial role in the energization of electrons since electrons can gain several tens of eV when crossing the double layer

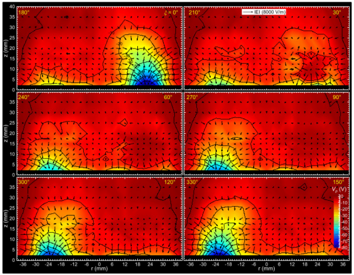

From Panjan and Anders (2017) JAP **121** 063302

Electron power absorption

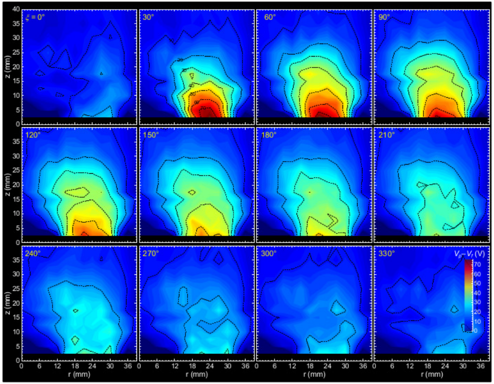

From Panjan and Anders (2017) JAP **121** 063302

- The distribution of $V_\mathrm{p} - V_\mathrm{f} \propto \langle E \rangle$ in the $r - z$ plane for a dc magnetron sputtering discharge operated at 270 V and 0.27 Pa

Electron power absorption

- Electrons gain energy when they encounter an electric field – a potential gradient, such as the field in the double layer
- The electron heating power $\mathbf{J}_{\rm e} \cdot \mathbf{E}$ is associated with an acceleration of electrons in the electric field – this electron energization in a double layer is Ohmic heating

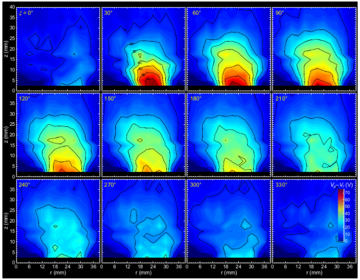

From Panjan and Anders (2017) JAP **121** 063302

The ionization region model (IRM)

Ionization region model

- The ionization region model (IRM) is a time-dependent volume averaged plasma chemical model of the ionization region (IR) of the HiPIMS discharge
- The IRM gives the temporal evolution of the densities of ions, neutrals and electrons
- The IRM gives also two internal parameters that are of importance
  - α_t – ionization probability
  - β_t – back-attraction probability

Detailed model description is given in Huo et al. (2017) JPD **50** 354003

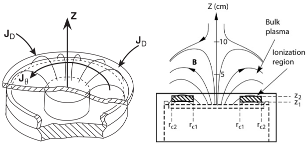

The definition of the volume covered by the IRM

- The IR is defined as an annular cylinder of width $w_{rt} = r_{c2} - r_{c1}$ and thickness $L = z_2 - z_1$, extends from z_1 to z_2 axially away from the target

From Raadu et al. (2011) PSST **20** 065007

Ionization region model

- The temporal development is defined by a set of ordinary differential equations giving the first time derivatives of
  - the electron energy
  - the particle densities for all the particles (except electrons)
- The species assumed in the non-reactive-IRM are
  - cold electrons e^{C}, hot electrons e^{H}
  - argon atoms Ar($3s^2 3p^6$), warm argon atoms in the ground state Ar^{W}, hot argon atoms in the ground state Ar^{H}, Ar^{m} ($1s_5$ and $1s_3$) (11.6 eV), argon ions Ar^{+} (15.76 eV), doubly ionized argon ions Ar^{2+} (27.63 eV)
  - Metal atoms, sometimes metastable states, metal ion M^{+}, and doubly ionized metal ions M^{2+}

Detailed model description is given in Huo et al. (2017) JPD **50** 354003

Ionization region model

- As an example the particle balance equation for the metal ion M^+ is

$$\frac{\mathrm{d}n_{\mathrm{M}^+}}{\mathrm{d}t} = \underbrace{k^{\mathrm{c}}_{\mathrm{iz,M}} n_{\mathrm{e,c}} n_{\mathrm{M}} + k^{\mathrm{h}}_{\mathrm{iz,M}} n_{\mathrm{e,h}} n_{\mathrm{M}}}_{\text{electron impact ionization}} + \underbrace{k_{\mathrm{P,iz}} n_{\mathrm{Ar^m}} n_{\mathrm{M}}}_{\text{Penning ionization}}$$

$$+ \underbrace{k_{\mathrm{chexc,1}} n_{\mathrm{M}} n_{\mathrm{Ar}^+} + k_{\mathrm{chexc,2}} n_{\mathrm{M}^{2+}} n_{\mathrm{Ar}}}_{\text{charge exchange}} - \underbrace{k^{\mathrm{c}}_{\mathrm{iz,M}^+} n_{\mathrm{e,c}} n_{\mathrm{M}^+} - k^{\mathrm{h}}_{\mathrm{iz,M}^+} n_{\mathrm{e,h}} n_{\mathrm{M}^+}}_{\text{electron impact ionization to create } \mathrm{M}^{2+}}$$

$$- \underbrace{\frac{\Gamma^{\mathrm{RT}}_{\mathrm{M}^+} + \Gamma^{\mathrm{BP}}_{\mathrm{M}^+}(S_{\mathrm{IR}} - S_{\mathrm{RT}})}{\mathcal{V}_{\mathrm{IR}}}}_{\text{ion flux out of the ionization region}}$$

Ionization region model

- The IRM is a semi-empirical discharge model and requires the measured discharge current and voltage waveforms as inputs
- The IRM has three unknown fitting parameters
  - the ion back-attraction probability for the metal ions $\beta_{\mathrm{t,pulse}}$ and gas ions $\beta_{\mathrm{g,pulse}}$
  - the potential drop across the IR $f = V_{\mathrm{IR}}/V_{\mathrm{D}}$
  - the electron recapture probability $r = 0.7$
- This leaves the $(\beta_{\mathrm{t,pulse}}, f)$ parameter space to be explored through the model fitting procedure – the blue zones in the fitting map indicate the smallest mean square error

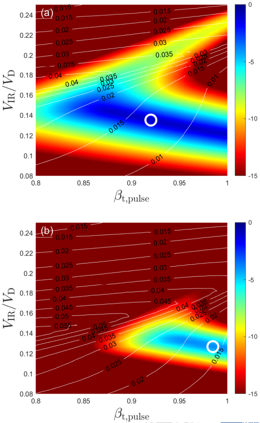

Graphite target from Eliasson et al. (2021) PSST **29** 115017

Ionization region model of HiPIMS

- The model is constrained by experimental data input and fitted to reproduce the measured discharge current and voltage curves, $I_{\mathrm{D}}(t)$ and $V_{\mathrm{D}}(t)$, respectively
- Two model fitting parameters were found to be sufficient for a discharge with Al target
  - V_{IR} accounts for the power transfer to the electrons
  - β is the probability of back-attraction of ions to the target

From Huo et al. (2017) JPD **50** 354003

Experimental data from Anders et al. (2007) JAP **102** 113303

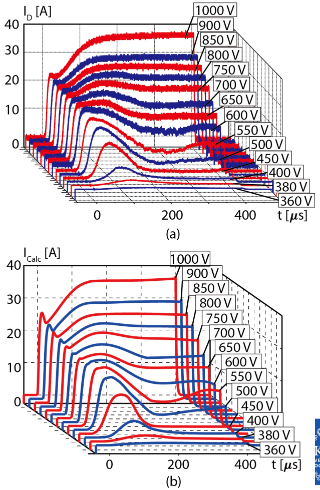

Ionization region model studies of HiPIMS discharges

Ionization region model studies of HiPIMS

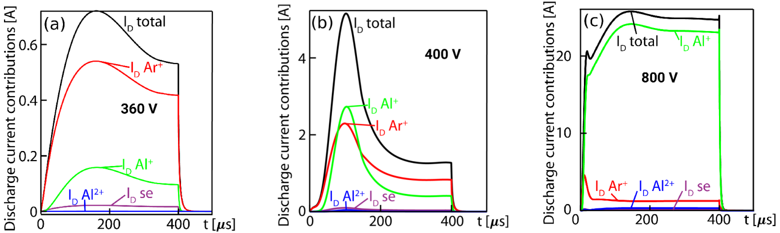

- A **non-reactive** discharge with 50 mm diameter Al target
- Current composition at the target surface

From Huo et al. (2017) JPD **50** 354003

Experimental data from Anders et al. (2007) JAP **102** 113303

Ionization region model studies of HiPIMS

- When the discharge is operated at 400 V the contributions of Al^+ and Ar^+-ions to the discharge current are very similar
- At 800 V Al^+-ions dominate the discharge current (**self-sputtering**) while the contribution of Ar^+ is below 10 % except at the initiation of the pulse

From Huo et al. (2017) JPD **50** 354003

Experimental data from Anders et al. (2007) JAP **102** 113303

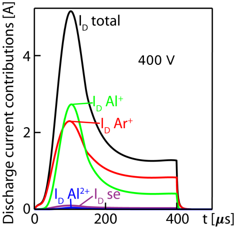

(a)

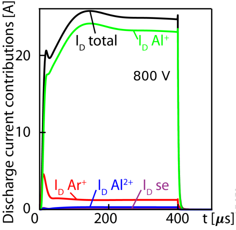

(b)

Ionization region model studies of HiPIMS

- A primary current $I_{\rm prim}$ is defined as ions of the working gas, here Ar^+, that are ionized for the first time and then drawn to the target
- This is the dominating current in dc magnetron sputtering discharges
- This current has a critical upper limit

$$I_{\rm crit} = S_{\rm RT} e p_{\rm g} \sqrt{\frac{1}{2\pi m_{\rm g} k_{\rm B} T_{\rm g}}} = S_{\rm RT} e n_{\rm g} \sqrt{\frac{k_{\rm B} T_{\rm g}}{2\pi m_{\rm g}}}$$

- Discharge currents $I_{\rm D}$ above $I_{\rm crit}$ are only possible if there is some kind of recycling of atoms that leave the target, become subsequently ionized and then are drawn back to the target

Anders et al. (2012) JPD **45** 012003

Huo et al. (2014) PSST **23** 025017

Ionization region model studies of HiPIMS

- For the 50 mm diameter Al target the critical current is $I_{\rm crit} \approx 7$ A
- The experiment is operated from far below $I_{\rm crit}$ to high above it, up to 36 A.
- With increasing current $I_{\rm prim}$ gradually becomes a very small fraction of the total discharge current $I_{\rm D}$
- The current becomes mainly carried by singly charged Al^+-ions, meaning that **self-sputter recycling** or the current $I_{\rm SS-recycle}$ dominates

From Huo et al. (2017) JPD **50** 354003

Experimental data from Anders et al. (2007) JAP **102** 113303

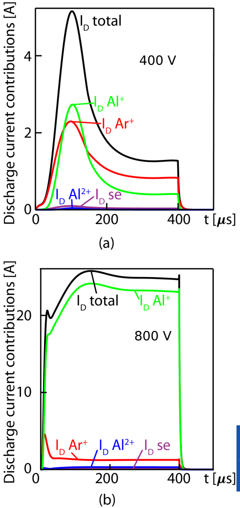

Ionization region model studies of HiPIMS

- For discharges with Ti target the peak current is far above the critical current (up to 650 A, while $I_{\rm crit} \approx 19$ A)
- However, this discharge shows close to a 50/50 combination of **self-sputter recycling** $I_{\rm SS-recycle}$ and **working gas-recycling** $I_{\rm gas-recycle}$
- Almost 2/3 of the current to the target is here carried by Ar^{+} and Ti^{2+}-ions, which both can emit secondary electrons upon target bombardment, and this gives a significant sheath energization

From Huo et al. (2017) JPD **50** 354003

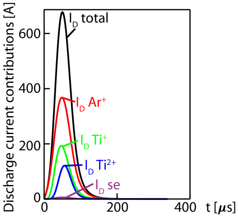

(a)

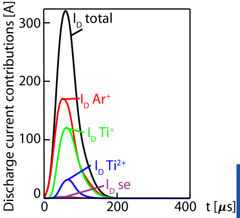

(b)

Ionization region model studies of HiPIMS

- **Reactive** HiPIMS
- Ar/O_2 discharge with Ti target
- For this system $I_{\mathrm{crit}} \approx 5$ A
- In the metal mode Ar^+ and Ti^+-ions contribute roughly equally to the current – combined **self-sputter recycling** and **working gas recycling**
- In the poisoned mode the current increaes and Ar^+-ions dominate the current – **working gas recycling**

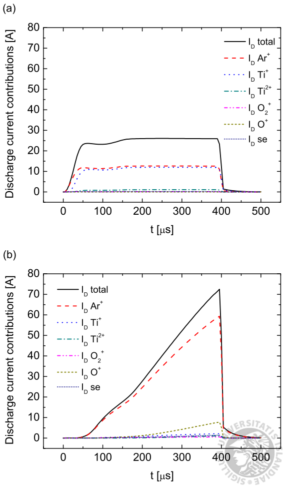

From Gudmundsson et al. (2016) PSST **25**(6) 065004

Ionization region model studies of HiPIMS

- The temporal evolution of the neutral and ion densities in a discharge with zirconium target
- Ar^+ ions dominate the discharge – but Zr^+ ions are not far off
- Ar^{2+} and Zr^{2+} ions have much lower densities
- Working gas rarefaction is very apparent

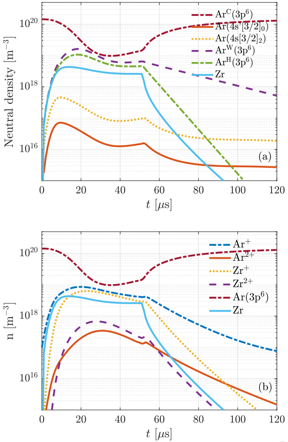

From Suresh Babu et al. (2024) JVSTA **42** 043007

Ionization region model studies of HiPIMS

- The temporal evolution of the neutral and ion densities in a discharge with graphite target
- Ar^+ ions dominate the discharge – constitute over 90% of the discharge current
- Working gas rarefaction is apparent
- The back-attraction probability is high $\beta_{t,pulse} > 0.83$

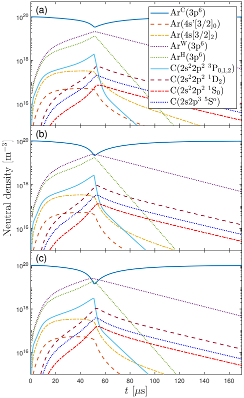

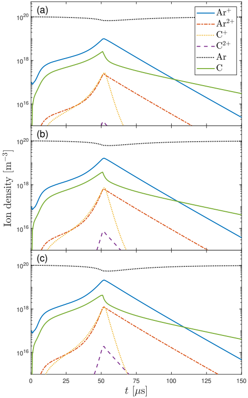

From Eliasson et al. (2021) PSST **29** 115017

Ionization region model studies of HiPIMS

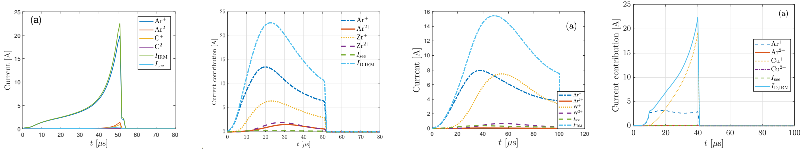

C: PSST (2021) **30** 115017 Zr: JVSTA (2024) **42** 043007 W: PSST (2022) **31** 065009 Cu: SCT (2022) **442** 128189

- The temporal evolution of the discharge current composition at the target surface for four different targets
- With Cu target Cu^+ ions dominate, with graphite target Ar^+ ions dominate
- For Zr and W targets there is a mix of Ar^+ and metal ions
- Note that the secondary electron current is very small

Ionization region model studies of HiPIMS

- Recall that singly charged metal ions cannot create the secondary electrons – for metal self-sputtering (γ_{SE} is practically zero)
- The first ionization energies of many metals are insufficient to overcome the workfunction of the target material
- For s discharge with Al or Cu target operated at high voltage, self-sputter dominated, the effective secondary electron emission is essentially zero

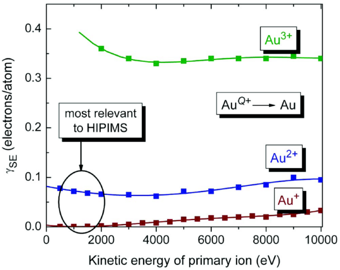

From Anders (2008) APL **92** 201501

Ionization region model studies of HiPIMS

- There are two mechanisms of electron power absorption
  - secondary electron acceleration across the sheath
  - Ohmic heating within the IR
- The power transfer to the electrons is given by

$$P_{\mathrm{e}} = P_{\mathrm{SH}} + P_{\mathrm{Ohm}} = I_{\mathrm{e,SH}} V_{\mathrm{SH}} + I_{\mathrm{e,IR}} V_{\mathrm{IR}}$$

  where

$$P_{\mathrm{Ohm}} = I_{\mathrm{e,IR}} V_{\mathrm{IR}} = \left\langle \frac{I_{\mathrm{e}}}{I_{\mathrm{D}}} \right\rangle I_{\mathrm{D}} V_{\mathrm{IR}}$$

  and $\langle I_{\mathrm{e}}/I_{\mathrm{D}} \rangle \sim 1/2$ is the volume average of the fraction of the discharge current in the IR that is carried by electrons
- The sheath potential is given by $V_{\mathrm{SH}} = V_{\mathrm{D}} - V_{\mathrm{IR}}$
- The sheath energization

$$P_{\mathrm{SH}} = I_{\mathrm{e,SH}} V_{\mathrm{SH}} = V_{\mathrm{SH}} \left(I_{\mathrm{Ar^+}} \gamma_{\mathrm{Ar^+,eff}} + \frac{1}{2} I_{\mathrm{Ar^{2+}}} \gamma_{\mathrm{Ar^{2+},eff}} + \frac{1}{2} I_{\mathrm{M^{2+}}} \gamma_{\mathrm{M^{2+},eff}} \right)$$

Ionization region model studies of HiPIMS

- For the Al target, Ohmic heating is in the range of 87 % (360 V) to 99 % (1000 V)
- The domination of Al^{+}-ions, which have zero secondary electron emission yield, has the consequence that there is negligible sheath energization
- The ionization threshold for twice ionized Al^{2+}, 18.8 eV, is so high that few such ions are produced

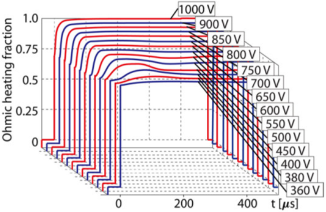

From Huo et al. (2017) JPD **50** 354003

Ionization region model studies of HiPIMS

- For a Ti target Ohmic heating is about 92 %
  - Both Ar^{+} and Ti^{2+}-ions contribute to creation of secondary electrons
- For Ti target in Ar/O_2 mixture
  - In the metal mode Ohmic heating is found to be 90 % during the plateau phase of the discharge pulse
  - For the poisoned mode Ohmic heating is 70 % with a decreasing trend, at the end of the pulse

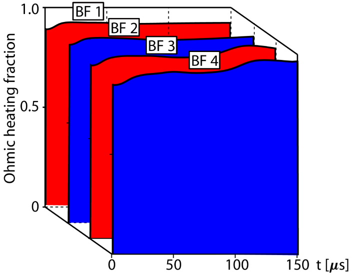

From Huo et al. (2017) JPD **50** 354003

Ionization region model studies of HiPIMS

- For a Cr target the Ohmic heating fraction depends on the pulse length, it increases with increased pulse length
- The Ohmic heating fraction also increases with increased peak discharge current density
- For a discharge with titanium target the share of Ohmic heating to be 70 % – 60 %, decreasing with decreasing magnetic field strength

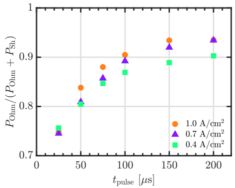

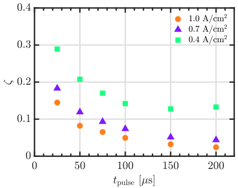

From Barynova et al. (2025) PSST to be submitted

Ionization region model studies of HiPIMS

- Ohmic heating is also very significant in dc magnetron sputtering discharges
- The relative contributions to the total ionization $\iota_{\rm total}$ due to Ohmic heating, $\iota_{\rm Ohmic}$, and sheath energization, $\iota_{\rm sheath}$
- A blue circle marks the HiPIMS study modelled by Huo et al. (2013)
- Note that this HiPIMS case $\gamma_{\rm SE,eff}$ is consistent with the dcMS cases

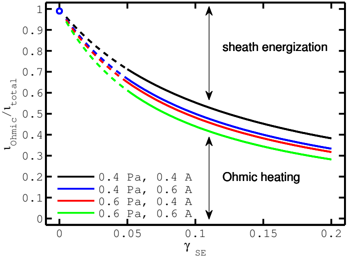

From Brenning et al. (2016) PSST **25** 065024

Deposition rate vs ionized flux fraction

Deposition rate vs ionized flux fraction – α_t and β_t

- We can relate the measured quantities normalized deposition rate $F_{DR,sput}$ and the ionized flux fraction $F_{ti,flux}$

$$F_{DR,sput} = \frac{\Gamma_{DR}}{\Gamma_0} = (1 - \alpha_t \beta_t)$$

$$F_{ti,flux} = \frac{\Gamma_{DR,ions}}{\Gamma_{DR,sput}} = \frac{\Gamma_0 \alpha_t (1 - \beta_t)}{\Gamma_0 (1 - \alpha_t \beta_t)} = \frac{\alpha_t (1 - \beta_t)}{(1 - \alpha_t \beta_t)}$$

to the internal parameters back attraction probability β_t

$$\beta_t = \frac{1 - F_{DR,sput}}{1 - F_{DR,sput}(1 - F_{ti,flux})}$$

and ionization probability α_t

$$\alpha_t = 1 - F_{DR,sput}(1 - F_{ti,flux})$$

Hajihoseini et al. (2019) *Plasma* **2** 201 and later refined by Rudolph et al. (2021) JAP **129** 033303

Deposition rate vs ionized flux fraction – α_t and β_t

- There are two measures of how good a HiPIMS discharge is:
  - the fraction $F_{DR,sput}$ of all the sputtered material that reaches the diffusion region (DR)
  - the fraction $F_{ti,flux}$ of ionized species in that flux
- There is a trade off between the goals of higher $F_{DR,sput}$ and higher $F_{ti,flux}$

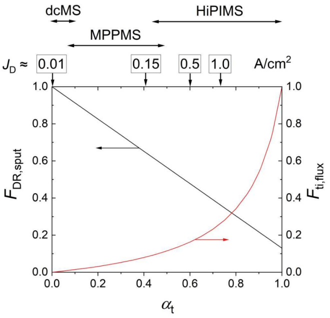

From Brenning et al. (2020) *JVSTA* **38** 033008

Deposition rate vs ionized flux fraction – α_t and β_t

- For a particular application an ionized flux fraction of 30 % is suitable
- For $\beta_t = 0.95$ following the green dotted line from the value $F_{ti,flux} = 0.30$ to the red dashed curve gives $\alpha_t = 0.9$ (red square)
- The black dashed line then shows that at this value of α_t only 15 % of the total sputtered flux enters the diffusion region ($F_{DR,sput} = 0.15$)

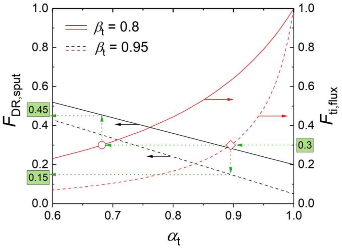

From Brenning et al. (2020) *JVSTA* **38** 033008

Deposition rate vs ionized flux fraction – α_t and β_t

- If the back-attraction can be reduced to $\beta_t = 0.8$ the deposition rate is increased
- The solid lines show that reducing the back-attraction to $\beta_t = 0.8$ where $\alpha_t = 0.69$ is sufficient to maintain $F_{ti,flux} = 0.30$ (red circle) $F_{DR,sput} = 0.45$ or a factor of three increase in the deposition rate

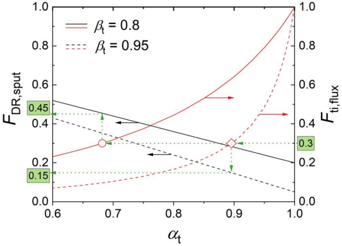

From Brenning et al. (2020) JVSTA **38** 033008

- The question that remains:
  - How can we vary the ionization probability α_t and maybe more importantly the back-attraction probability β_t ?

Deposition rate vs ionized flux fraction – α_t and β_t

- The internal discharge parameters α_t and β_t from the ionization region model (IRM)
- For tungsten target the ionization probability α_t increases with increased discharge voltage or increased discharge current density
- The peak discharge current increases with increased discharge voltage
- The back-attraction probability $\beta_{t,pulse}$ decreases with increased discharge voltage

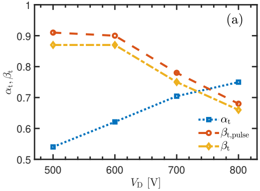

A discharge with a tungsten target

From Suresh Babu et al. (2022) PSST **31** 065009

Deposition rate vs ionized flux fraction – α_t and β_t

- For zirconium target the ionization probability α_t increases with increased current density
- The back-attraction probability $\beta_{t,pulse}$ does not show any trend

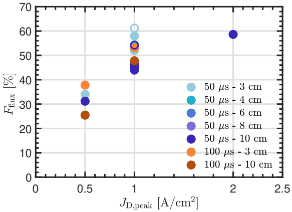

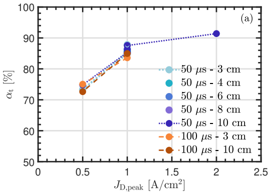

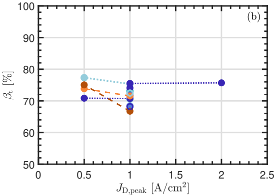

- The measured ionized flux fraction is used to lock the model

discharge with a zirconium target

From Suresh Babu et al. (2024) JVSTA **42** 043007

Deposition rate vs ionized flux fraction – α_t and β_t

- For chromium target the ionization probability α_t increases with increased discharge current density
- The back-attraction probability $\beta_{t,pulse}$ decreases with increased peak discharge current density and with decreasing pulse length

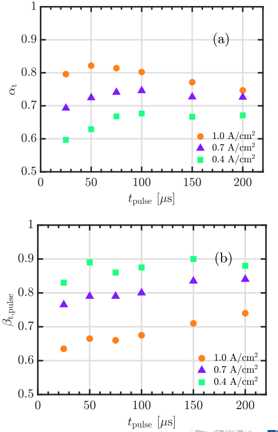

From Barynova et al. (2025) PSST to be submitted

Deposition rate vs ionized flux fraction – α_t and β_t

- The ionization probability α_t increases with increased discharge current

From Rudolph et al. (2022) JPD **55** 015202

- The ion escape fraction $(1 - \beta_t)$ versus the magnetic field strength

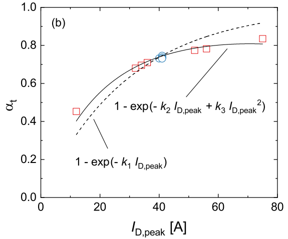

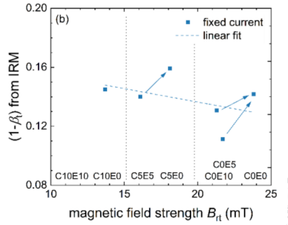

Deposition rate vs ionized flux fraction – α_t *and* β_t

- We know that the electron temperature and the hot electron density fall with increased sputter yield
- Held *et al.* observed that titanium atoms are ionized within 0.5 mm from the target surface (high $\beta_{t,\text{pulse}}$), while aluminum and chromium atoms can travel further before being ionized (lower $\beta_{t,\text{pulse}}$)
- The measured electron temperature is 4.5 eV for titanium target compared to 2.6 eV (aluminum) and 1.5 eV (chromium)

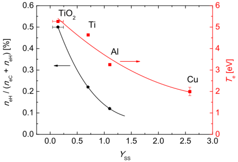

From Brenning et al. (2017) PSST **26** 125003

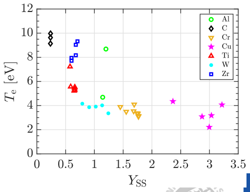

From Barynova et al. (2025) PSST submitted

Held et al. (2023) PSST **32** 065002

Deposition rate vs ionized flux fraction – α_t and β_t

- What determines the back-attraction probability ?
- How can one influence the back-attraction probability ?
- The back-attraction probability $\beta_{t,pulse}$, determined by IRM, versus the self-sputter yield for various target materials
- The data indicate that the back-attraction probability decreases roughly linearly with increased self-sputter yield

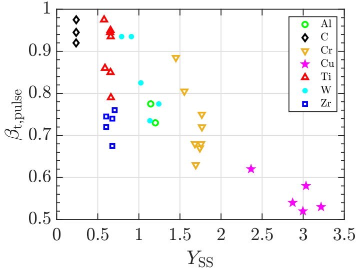

From Barynova et al. (2025) PSST submitted

Working gas rarefaction

Working gas rarefaction

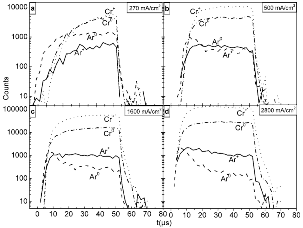

From Alami et al. (2006) APL **89**(15) 154104

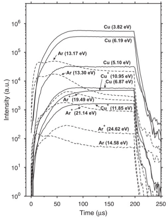

From Vlček et al. (2004) Contrib. Plasma Phys. **44** 426

- The sputtered species enter the discharge at considerable energy, which is determined by the cohesive energy of the solid target
- The interaction between the energetic sputtered particles and the working gas atoms can lead to a reduction in the working gas density – as has been observed experimentally in the HiPIMS discharge

Working gas rarefaction

- HiPIMS discharge with graphite target and $J_{\mathrm{D,peak}} = 1$ A cm^{-2}

  Eliasson et al. (2021) PSST **30** 115017

- Argon atoms are lost mainly through electron impact ionization by primary and secondary electrons
- Contributions of kick-out and charge-exchange are negligible
- Diffusion contributes to a net loss of argon atoms during the pulse, but to a flow into the ionization region after the pulse is off

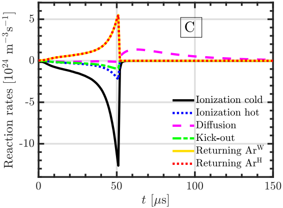

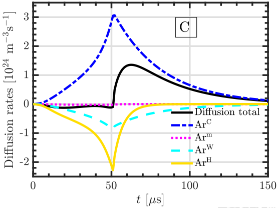

From Barynova et al. (2024) PSST **33**(6) 065010

Working gas rarefaction

- HiPIMS discharge with tungsten target and $J_{\mathrm{D,peak}} = 0.54$ A cm^{-3}

  Suresh Babu et al. (2022) PSST **31** 065009

- The main contributor to the loss of argon atoms from the IR is kick-out by tungsten atoms sputtered from the target (39 – 48 % contribution)

- The second most important loss process is electron impact ionization by secondary electrons followed by electron impact ionization by the primary electrons

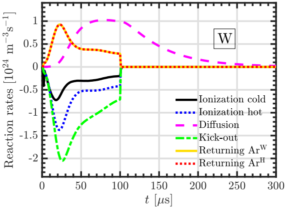

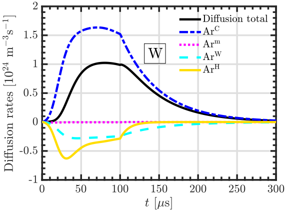

From Barynova et al. (2024) PSST **33**(6) 065010

Working gas rarefaction

- The relative contributions of the various processes to working gas rarefaction varies greatly depending on the target material for $J_{\mathrm{D,peak}} \sim 1$ A/cm^2 and $p_{\mathrm{g}} \sim 1$ Pa
- For targets with low sputter yield electron impact ionization is the dominating process
- For high sputter yield target materials kick-out of argon atoms by the metal atoms is the dominating process
- The sputter yield is the primary factor that dictates which process is the most important for working gas rarefaction

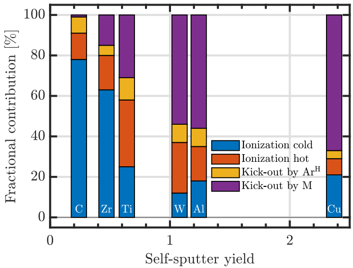

From Barynova et al. (2024) PSST **33**(6) 065010

Summary

- It has been demonstrated that Ohmic heating of the electrons can play a significant role in conventional dc magnetron sputtering discharges
- The discharge current composition at the target surface depends on the target material
- There is an inescapable conflict between the goals of higher deposition rate and higher fraction of ionized species in the sputtered material flux
- The back-attraction probability appears to depend on the self-sputter yield – it is lower for higher self-sputter yield
- The main contributor to working gas rarefaction for low sputter yield target is electron impact ionization, while for targets with high sputter yield kick-out by the sputtered species is the main contributor

Thank you for your attention

The slides can be downloaded at

`http://langmuir.raunvis.hi.is/~tumi/ranns.html`

The work has been in collaboration with

Dr. Daniel Lundin, Linköping University, Linköping, Sweden
Prof. Nils Brenning, KTH Royal Institite of Technology, Stockholm, Sweden
Prof. Ulf Helmersson, Linköping University, Linköping, Sweden
Dr. Martin Rudolph, Leibniz Institute of Surface Engineering (IOM), Leipzig, Germany
Prof. Tetsuhide Shimizu, Tokyo Metropolitan University, Tokyo, Japan
Dr. Michael A. Raadu, KTH Royal Institite of Technology, Stockholm, Sweden
Prof. Tiberu Minea, Université Paris-Sud, Orsay, France
Dr. Hamidreza Hajihoseini, Dutch Institute for Fundamental Energy Research, Eindhoven, The Netherlands
Dr. Swetha Suresh Babu, University of Iceland, Reykjavik, Iceland
Joel Fischer, Linköping University, Linköping, Sweden
Kateryna Barynova, University of Iceland, Reykjavik, Iceland

References

Alami, J., K. Sarakinos, G. Mark, and M. Wuttig (2006). On the deposition rate in a high power pulsed magnetron sputtering discharge. *Applied Physics Letters 89*(15), 154104.

Anders, A. (2008). Self-sputtering runaway in high power impulse magnetron sputtering: The role of secondary electrons and multiply charged metal ions. *Applied Physics Letters 92*(20), 201501.

Anders, A. (2011). Discharge physics of high power impulse magnetron sputtering. *Surface and Coatings Technology 205*, S1–S9.

Anders, A., J. Andersson, and A. Ehiasarian (2007). High power impulse magnetron sputtering: Current-voltage-time characteristics indicate the onset of sustained self-sputtering. *Journal of Applied Physics 102*(11), 113303.

Anders, A., J. Čapek, M. Hála, and L. Martinu (2012). The 'recycling trap': a generalized explanation of discharge runaway in high-power impulse magnetron sputtering. *Journal of Physics D: Applied Physics 45*(1), 012003.

Barynova, K., N. Brenning, S. Suresh Babu, J. Fischer, D. Lundin, M. A. Raadu, J. T. Gudmundsson, and M. Rudolph (2025). Self-regulating electron temperature in high-power impulse magnetron sputtering discharges and its effect on the metal ion escape. *Plasma Sources Science and Technology*, submitted for publication.

Barynova, K., T. Shimizu, M. Zanáška, R. P. B. Viloan, M. Rudolph, D. Lundin, and J. T. Gudmundsson (2025). High power impulse magnetron sputtering of a chromium target. *Plasma Sources Science and Technology*, to be sbmitted for publication.

Barynova, K., S. Suresh Babu, M. Rudolph, J. Fischer, D. Lundin, M. A. Raadu, N. Brenning, and J. T. Gudmundsson (2024). On working gas rarefaction in high power impulse magnetron sputtering. *Plasma Sources Science and Technology 33*(6), 065010.

Bohlmark, J., J. T. Gudmundsson, J. Alami, M. Lattemann, and U. Helmersson (2005). Spatial electron density distribution in a high-power pulsed magnetron discharge. *IEEE Transactions on Plasma Science 33*(2), 346–347.

Bohlmark, J., M. Lattemann, J. T. Gudmundsson, A. P. Ehiasarian, Y. A. Gonzalvo, N. Brenning, and U. Helmersson (2006). The ion energy distributions and ion flux composition from a high power impulse magnetron sputtering discharge. *Thin Solid Films 515*(5), 1522–1526.

Brenning, N., J. T. Gudmundsson, D. Lundin, T. Minea, M. A. Raadu, and U. Helmersson (2016). The role of ohmic heating in dc magnetron sputtering. *Plasma Sources Science and Technology 25*(6), 065024.

References

Brenning, N., J. T. Gudmundsson, M. A. Raadu, T. J. Petty, T. Minea, and D. Lundin (2017). A unified treatment of self-sputtering, process gas recycling, and runaway for high power impulse sputtering magnetrons. *Plasma Sources Science and Technology 26*(12), 125003.

Brenning, N., A. Butler, H. Hajihoseini, M. Rudolph, M. A. Raadu, J. T. Gudmundsson, T. Minea, and D. Lundin (2020). Optimization of HiPIMS discharges: The selection of pulse power, pulse length, gas pressure, and magnetic field strength. *Journal of Vacuum Science and Technology A 38*(3), 033008.

Depla, D., S. Mahieu, and R. De Gryse (2009). Magnetron sputter deposition: Linking discharge voltage with target properties. *Thin Solid Films 517*(9), 2825–2839.

Eliasson, H., M. Rudolph, N. Brenning, H. Hajihoseini, M. Zanáška, M. J. Adriaans, M. A. Raadu, T. M. Minea, J. T. Gudmundsson, and D. Lundin (2021). Modeling of high power impulse magnetron sputtering discharges with graphite target. *Plasma Sources Science and Technology 30*(11), 115017.

Gudmundsson, J. T. (2008). Ionized physical vapor deposition (IPVD): Magnetron sputtering discharges. *Journal of Physics: Conference Series 100*, 082002.

Gudmundsson, J. T. (2016). On reactive high power impulse magnetron sputtering. *Plasma Physics and Controlled Fusion 58*(1), 014002.

Gudmundsson, J. T., J. Alami, and U. Helmersson (2002). Spatial and temporal behavior of the plasma parameters in a pulsed magnetron discharge. *Surface and Coatings Technology 161*(2-3), 249–256.

Gudmundsson, J. T., N. Brenning, D. Lundin, and U. Helmersson (2012). The high power impulse magnetron sputtering discharge. *Journal of Vacuum Science and Technology A 30*(3), 030801.

Gudmundsson, J. T., D. Lundin, N. Brenning, M. A. Raadu, C. Huo, and T. M. Minea (2016). An ionization region model of the reactive Ar/O_2 high power impulse magnetron sputtering discharge. *Plasma Sources Science and Technology 25*(6), 065004.

Hajihoseini, H. and J. T. Gudmundsson (2017). Vanadium and vanadium nitride thin films grown by high power impulse magnetron sputtering. *Journal of Physics D: Applied Physics 50*(50), 505302.

Held, J., V. Schulz-von der Gathen, and A. von Keudell (2023). Ionization of sputtered material in high power impulse magnetron sputtering plasmas – comparison of titanium, chromium and aluminum. *Plasma Sources Science and Technology 32*(6), 065006.

References

Gudmundsson, J. T. (2020). Physics and technology of magnetron sputtering discharges. *Plasma Sources Science and Technology 29*(11), 113001.

Gudmundsson, J. T. and D. Lundin (2020). Introduction to magnetron sputtering. In D. Lundin, T. Minea, and J. T. Gudmundsson (Eds.), *High Power Impulse Magnetron Sputtering: Fundamentals, Technologies, Challenges and Applications*, pp. 1–48. Amsterdam, The Netherlands: Elsevier.

Hajihoseini, H., M. Čada, Z. Hubička, S. Ünaldi, M. A. Raadu, N. Brenning, J. T. Gudmundsson, and D. Lundin (2019). The effect of magnetic field strength and geometry on the deposition rate and ionized flux fraction in the HiPIMS discharge. *Plasma 2*(2), 201–221.

Huo, C., D. Lundin, J. T. Gudmundsson, M. A. Raadu, J. W. Bradley, and N. Brenning (2017). Particle-balance models for pulsed sputtering magnetrons. *Journal of Physics D: Applied Physics 50*(35), 354003.

Huo, C., D. Lundin, M. A. Raadu, A. Anders, J. T. Gudmundsson, and N. Brenning (2013). On sheath energization and ohmic heating in sputtering magnetrons. *Plasma Sources Science and Technology 22*(4), 045005.

Huo, C., D. Lundin, M. A. Raadu, A. Anders, J. T. Gudmundsson, and N. Brenning (2014). On the road to self-sputtering in high power impulse magnetron sputtering: particle balance and discharge characteristics. *Plasma Sources Science and Technology 23*(2), 025017.

Kateb, M., H. Hajihoseini, J. T. Gudmundsson, and S. Ingvarsson (2019). Role of ionization fraction on the surface roughness, density, and interface mixing of the films deposited by thermal evaporation, dc magnetron sputtering, and HiPIMS: An atomistic simulation. *Journal of Vacuum Science and Technology A 37*(3), 031306.

Panjan, M. and A. Anders (2017). Plasma potential of a moving ionization zone in DC magnetron sputtering. *Journal of Applied Physics 121*(6), 063302.

Raadu, M. A., I. Axnäs, J. T. Gudmundsson, C. Huo, and N. Brenning (2011). An ionization region model for high power impulse magnetron sputtering discharges. *Plasma Sources Science and Technology 20*(6), 065007.

Rudolph, M., H. Hajihoseini, M. A. Raadu, J. T. Gudmundsson, N. Brenning, T. M. Minea, A. Anders, and D. Lundin (2021). On how to measure the probabilities of target atom ionization and target ion back-attraction in high-power impulse magnetron sputtering. *Journal of Applied Physics 129*(3), 033303.

References

Rudolph, M., N. Brenning, H. Hajihoseini, M. A. Raadu, T. M. Minea, A. Anders, D. Lundin, and J. T. Gudmundsson (2022). Influence of the magnetic field on the discharge physics of a high power impulse magnetron sputtering discharge. *Journal of Physics D: Applied Physics 55*(1), 015202.

Samuelsson, M., D. Lundin, J. Jensen, M. A. Raadu, J. T. Gudmundsson, and U. Helmersson (2010). On the film density using high power impulse magnetron sputtering. *Surface and Coatings Technology 202*(2), 591–596.

Suresh Babu, S., M. Rudolph, D. Lundin, T. Shimizu, J. Fischer, M. A. Raadu, N. Brenning, and J. T. Gudmundsson (2022). Ionization region model of a high power impulse magnetron sputtering of tungsten. *Plasma Sources Science and Technology 31*(6), 065009.

Suresh Babu, S., J. Fischer, M. Rudolph, D. Lundin, and J. T. Gudmundsson (2024). Modeling of high power impulse magnetron sputtering discharges with a zirconium target. *Journal of Vacuum Science and Technology A 42*(4), 043007.

Thornton, J. A. (1978). Magnetron sputtering: basic physics and application to cylindrical magnetrons. *Journal of Vacuum Science and Technology 15*(2), 171–177.

Vlček, J., A. D. Pajdarová, and J. Musil (2004). Pulsed dc magnetron discharges and their utilization in plasma surface engineering. *Contributions to Plasma Physics 44*(5-6), 426–436.